232 Vol. 4, No. 3 / 25 June 2026 / *Optica Quantum* Research Article

OPTICA QUANTUM

Multi-laser stabilization with an atomic-disciplined photonic integrated resonator

Andrei Isichenko,[1] Andrew S. Hunter,[1] Nitesh Chauhan,[1] John R. Dickson,[2] T. Nathan Nunley,[3,4] Josiah R. Bingaman,[2] David A. S. Heim,[1] Mark W. Harrington,[1] Kaikai Liu,[1] Paul D. Kunz,[2,4] and Daniel J. Blumenthal[1,*]

[1]Department of Electrical and Computer Engineering, University of California Santa Barbara, Santa Barbara, California 93106, USA
[2]Department of Physics, Center of Complex Quantum Systems, The University of Texas at Austin, Austin, Texas 78712, USA
[3]General Technical Services, 1451 NJ-34, Wall Township, New Jersey 07727, USA
[4]DEVCOM Army Research Laboratory South, Austin, Texas 78712, USA
*danb@ucsb.edu

Received 29 August 2025; revised 12 March 2026; accepted 31 March 2026; published 24 April 2026

Precision atomic and quantum experiments rely on ultra-stable narrow linewidth lasers constructed using table-top ultra-low expansion reference cavities. These experiments often require multiple lasers, operating at different wavelengths, to perform key steps used in state preparation and measurement required in quantum sensing and computing. This is traditionally achieved by disciplining a cavity-stabilized laser to a key atomic transition and then transferring the transition linewidth and stability to other lasers using the same reference cavity in combination with bulk-optic frequency shifting such as acousto-optic modulators. Transitioning such capabilities to a future potentially low-cost photonic-integrated platform will enable a wide range of portable, low power, scalable quantum experiments and applications. Yet, today's bulk optic approaches pose challenges related to lack of cavity tunability, large free spectral range, and limited photonic integration potential. Here, we address these challenges with demonstration of an agile photonic-integrated 780 nm ultra-high-Q tunable silicon nitride reference cavity that performs multiple critical experimental steps including laser linewidth narrowing, high resolution rubidium spectroscopy, dual-stage stabilization to a rubidium transition, and stability transfer to other lasers. We achieve up to 20 dB of frequency noise reduction at 10 kHz offset, precision spectroscopy over a 250 MHz range, and dual-stage locking to rubidium with an Allan deviation of 8.5×10^{-12} at 1 s and up to 40 dB frequency noise reduction at 100 Hz frequency offset. We further use the rubidium-disciplined cavity to provide atomic-referenced frequency stability to a second laser and demonstrate multi-wavelength Rydberg electrometry quantum sensing. These results pave the path for integrated, compact, and scalable solutions for quantum sensing, computing, and other atomic and trapped ion applications.

https://doi.org/10.1364/OPTICAQ.577668

1. INTRODUCTION

Atomically disciplined lasers are critical for next-generation precision applications including quantum sensing [1], quantum computing [2,3], navigation [4], and timekeeping [5]. These applications require lasers with low frequency noise and stabilization to an atomic energy transition. The disciplining of lasers to an atom or trapped-ion enables applications such as optical atomic clocks [6], high-fidelity neutral atom sensors and computers [2,3] or trapped-ion qubits [7], and key supporting functions such as atomic spectroscopy [8] and qubit state preparation and measurement (SPAM) [7]. In particular, quantum applications such as Rydberg electrometry [9–11] require the simultaneous stabilization of multiple laser frequencies to atomic transitions or relative to a main transition. This is achieved by Pound–Drever–Hall (PDH) locking each laser to one or more low-drift ultra-low expansion (ULE), high-finesse bulk-optic reference cavities [12], by using atomic spectroscopy in combination with a tunable or scanning cavity as a transfer cavity [13], or by using a fiber frequency comb system. In the latter approach, the transfer cavity is locked to an atom-referenced laser, and the resulting stability is transferred to additional lasers locked to the nearest cavity resonances. Tunable high-finesse transfer cavities (THFTCs) have also been demonstrated for linewidth narrowing, including stabilization of 780 nm and 960 nm lasers for single-atom coherent Rydberg excitations (10 kHz integral linewidths, 22 kHz long-term drift) [14]. Related work has demonstrated piezoelectrically tunable ultra-stable optical cavities capable of 120 kHz modulation

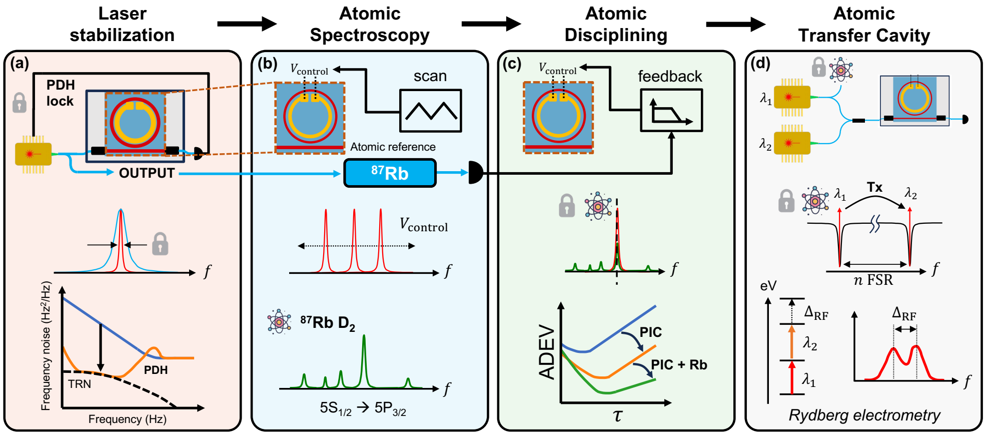

Fig. 1. Overview of the photonic-integrated ultra-high-Q (UHQ) resonator reference cavity and its application to atomic laser stabilization and multi-laser transfer cavity locking. (a) A 780 laser is Pound–Drever–Hall (PDH) locked to the integrated resonator, reducing its frequency noise to the cavity thermo-refractive noise limit (TRN) and causing the laser to closely track the resonator. (b) The same PIC resonator is thermally tuned causing the laser to scan across the rubidium D2 absorption spectrum. (c) Once aligned, feedback from the Rb spectroscopy signal is applied to the thermal tuner, implementing dual-stage locking. This disciplines the resonator frequency to the absolute atomic reference, improving long-term frequency stability as illustrated by the reduced Allan deviation (ADEV). (d) The stabilized resonator acts as a transfer cavity to lock multiple lasers, transferring the atomic stability to the second laser. This enables precise alignment of excitation lasers used in rubidium Rydberg electrometry, where a separate rubidium cell is used to detect RF signals via the measured Autler–Townes splitting (Δ_{RF}).

and fractional frequency stability approaching 10^{-14}, enabling transfer-cavity stabilization with extremely low drift [15]. With ULE cavities, given the large FSR, frequency shifting is employed to fill the frequency gap between the available cavity modes and the desired atomic transitions using an electro-optic modulator (EOM) or an acousto-optic modulator (AOM) and offset sideband [16] or offset beat-note locking [17]. Tuning of the cavity reduces the need for bulk frequency shifters; however, table-top ULE reference cavities are not always tunable and do not lend easily to integration. The tunability of the reference cavity is therefore a key feature of this locking technique.

Recent advances in miniaturization of high quality factor (Q), high finesse reference cavities across multiple platforms [18–25] have provided progress toward these goals. Centimeter-scale microcavities [25] demonstrate short-term stability on the order of 10^{-13} at 1 second, yet have limited tunability and slow tuning speeds on the order of minutes as well as large FSRs over 10 GHz. Compact crystalline whispering gallery mode (WGM) resonators have demonstrated self-injection locking for strong short-term laser frequency stabilization and, when combined with piezoelectric actuation, two-stage rubidium spectroscopy locking for long-term stability at the 10^{-12} level [18,19]. Simultaneous stabilization of two lasers at diverse wavelengths has also been demonstrated [26,27]. While these approaches achieve excellent performance, their integration and scalability remain limited, relying on discrete micro-optics packaging and specialized crystalline fabrication. An important approach is the CMOS fabrication-compatible integrated low loss silicon nitride platform to fabricate coil and spiral resonators [23,28]. These resonators have significantly lower FSR owing to their meter-scale cavity lengths [23] and can be dynamically tuned using on-chip stress-optic [29–31] and thermal [32] actuators. However, such integrated tunable cavities have not yet been demonstrated for atomic spectroscopy, multi-wavelength atomic transfer cavity locking, or for stability transfer in quantum applications.

Here, we report a photonic-integrated approach to perform key steps used in the preparation and measurement of atomic states in quantum experiments. We demonstrate a tunable, integrated ultra-high-quality (UHQ) factor silicon nitride resonator cavity that simultaneously performs laser linewidth narrowing and frequency noise reduction, rubidium atomic spectroscopy, dual-stage laser locking to the rubidium D_2 transition, and functions as a multi-laser transfer cavity lock for a Rydberg RF electrometry demonstration. The cavity is a silicon nitride ring resonator with a Q factor of 130 million, finesse 982, and a thermal actuator that can continuously tune the resonance with an efficiency of 19 MHz/mW. We stabilize a 780 nm semiconductor laser via PDH locking to the integrated cavity and perform spectroscopy by actuating the thermal tuner and sweeping the linewidth narrowed 780 nm laser over the full rubidium hyperfine transition range. We then simultaneously stabilize the laser and integrated cavity to the rubidium D_2 line using a dual stage PDH lock, achieving up to 4 orders magnitude close-to-carrier frequency noise reduction, reduction of the laser integral linewidth from 5 MHz to 326 kHz, and measure stabilization of 8.5×10^{-12} at 1 second—a two order of magnitude improvement compared to the 9×10^{-10} at 1 second by locking to the cavity only. Lastly, we use the transfer cavity locked to the rubidium D_2 transition to stabilize a 776 nm laser and demonstrate multi-wavelength Rydberg RF sensing. These results highlight the potential of photonic integrated tunable reference cavities to drive compact, scalable, and precise atomic and quantum systems.

2. RESONATOR FOR LASER LOCKING AND ATOMIC STABILIZATION

The working principle and functional stages are shown in Fig. 1. A commercial single-frequency 780 nm laser (Photodigm DBR) is Pound–Drever–Hall (PDH) locked to the cavity resonance for linewidth narrowing and frequency noise reduction, forming the first locking stage (Fig. 1(a)). Thermal tuning of the cavity enables frequency control of the locked laser (Fig. 1(b))

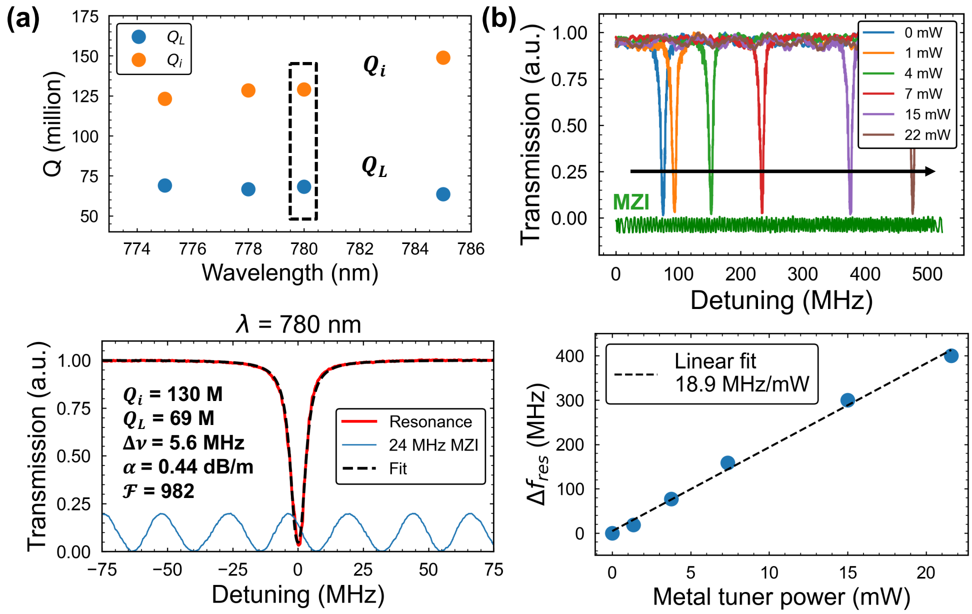

Fig. 2. Tunable integrated reference cavity characterization. (a) Intrinsic (Q_i) and loaded (Q_L) Q measurements for wavelengths near the rubidium 780 nm transition and transmission trace and fitting for a resonance at 780 nm achieving a loss α of 0.44 dB/m, total linewidth $\Delta\nu$ of 5.6 MHz, and finesse $\mathcal{F}$of 982. The frequency detuning is calibrated with an unbalanced Mach–Zehnder interferometer (MZI, blue trace). (b) Static tuning of the thermal actuator shows a high extinction ratio across the measured >400 MHz tuning range. Linear fit to extract the 19 MHz/mW thermal tuning coefficient of the resonance shift Δf_{res}.

and scanning the cavity allows for locating the rubidium spectroscopy peaks. In the second locking stage (Fig. 1(c)), the signal from the spectroscopy is fed back to the cavity tuner, stabilizing the PIC-locked laser to a hyperfine atomic transition and reducing the Allan deviation (ADEV) at longer averaging times. Lastly, the atom-stabilized resonator is used as a transfer cavity to lock multiple lasers to other cavity resonances, thereby transferring the stability from the reference laser to other lasers. In our work, this enables frequency stabilization of both 780 nm and 776 nm lasers for rubidium Rydberg electrometry, where the Autler–Townes splitting is used to detect radiofrequency (RF) electric fields as a quantum sensor.

A. Resonator Characterization

The integrated cavity consists of a fiber pigtailed, ultra-high-Q SiN ring resonator with a thermal tuner, fabricated on a 200 mm wafer from a CMOS foundry [33]. We characterize the resonator quality factor and tuning in Fig. 2. The resonator intrinsic Q_i = 130 M and loaded Q_L = 69 M for the TM_0 mode are measured using an unbalanced Mach–Zehnder interferometer (MZI) [24,34] resulting in a linewidth of 5.6 MHz and a loss of 0.44 dB/m (Fig. 2(a)). The ring resonator radius is 5.84 mm corresponding to a 5.5 GHz free-spectral range (FSR) and a finesse $\mathcal{F}$ = 982. We measure the relative resonance shift as a function of power applied to the thermal tuner as shown in Fig. 2(b) yielding a linear tuning coefficient of 19 MHz/mW. The measured tuning range of over 400 MHz is sufficient to cover the rubidium D_2 line spectroscopy peaks (within a single hyperfine manifold) for SAS [35]. The device design and fabrication details are provided in Note 1 and Fig. S1 of Supplement 1.

B. Laser Frequency Stabilization

The integrated high-Q resonator cavity enables strong frequency noise reduction of a 780-nm semiconductor laser using PDH locking. We package the resonator with polarization-maintaining (PM) fibers and internal temperature control for stable, plug-and-play locking with single-frequency 780 nm lasers. In this experiment, we used a 780-nm Distributed Bragg Reflector laser (DBR, Photodigm) and a Velocity TLB-6730-P tunable external cavity diode laser (ECDL, Newport) with a tuning range of 765–781 nm. We characterize the laser frequency noise using a fiber MZI optical frequency discriminator (OFD) [24].

We generate the error signal for PDH locking by monitoring the resonator transmission port fiber output on a photodetector and applying a 15.1 MHz modulation to either the laser current or by using a commercial electro-optic phase modulator (EOPM). The error signal is fed into a PID loop filter and the control signal is sent to the laser current control port (Fig. 3(a), top). The stabilized output is taken after a fiber splitter tap after the laser isolator. This PDH lock requires a minimum of 2 mW going into the packaged reference cavity, allowing for 90% of the laser output available for subsequent experiments requiring frequency-stabilized light. We implement the lock with both the DBR and ECDL lasers which have different free-running fundamental (FLW) and integral linewidths (ILW). The OFD frequency noise (FN) measurement results for the PDH locking are shown in Fig. 3(b). At 10 kHz frequency offset, the PDH lock reduces the laser FN by 21 dB and 22 dB for the DBR and ECDL, respectively. The lock with the lower-noise ECDL laser achieves an ILW reduction from 23 kHz to 2 kHz and exhibits thermo-refractive noise (TRN) limited performance at 4–30 kHz frequency offsets. The free-running and locked laser linewidths are summarized in Table 1 and we discuss the PDH loop details in Note 2 and Fig. S2 of Supplement 1. In general, using a laser with a lower FLW and sufficient frequency modulation bandwidth enables tighter PDH locking and reduced ILW. Recent demonstrations of photonic-integrated external cavity

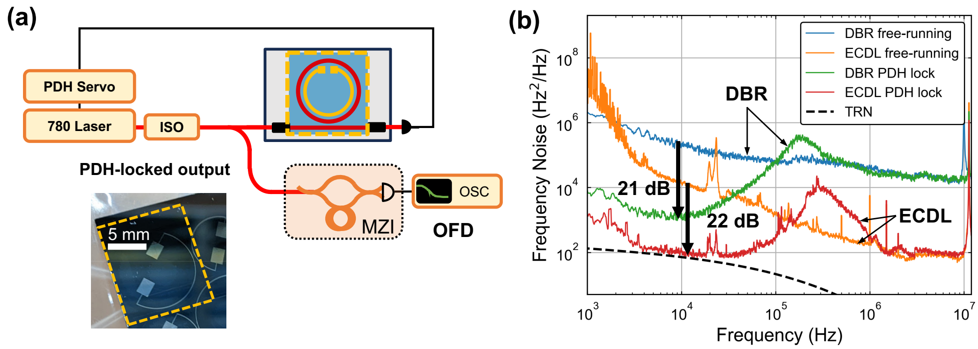

Fig. 3. Laser frequency stabilization to the tunable reference cavity. (a) Schematic for Pound–Drever–Hall (PDH) locking in the integrated resonator cavity. ISO, optical isolator; OFD, optical frequency discriminator. Inset: Photo of the metallized resonator cavity. (b) Laser frequency noise measurements with the OFD for the DBR laser and the ECDL laser. TRN, thermo-refractive noise.

Table 1. Laser Linewidths Achieved with Packaged Tunable PIC Stabilization

Configuration	$1/\pi$ ILW	β-Separation ILW	ILW Range
DBR, free-running	182 kHz[a]	5.1 MHz	0.1 Hz to 8 MHz
DBR, PIC lock	246 kHz[a]	306 kHz	0.1 Hz to 8 MHz
ECDL, free-running	23 kHz	354 kHz	1 kHz to 8 MHz
ECDL, PIC lock	1.5 kHz	2.3 kHz	1 kHz to 8 MHz
PIC TRN-limited	316 Hz	470 Hz	0.1 Hz to 8 MHz

[a]The increase in the locked $1/\pi$ ILW for the DBR is due to the location of the servo bump, which arises from limited phase margin in the feedback loop. Combined with the high fundamental linewidth of the laser (33 kHz) and the limited PDH loop gain, this places stricter requirements on the ability of the servo to suppress mid-range frequency noise (see Supplement 1, Note 2).

tunable lasers (ECTLs) with agile tuning capabilities [31], as well as locking a low-noise ECTL to a low-TRN coil resonator [36], have achieved sub-kHz ILW performance in the C-band.

C. Stabilized Laser Tuning and Modulation

Precise frequency tuning and dynamic modulation of the locked laser are essential for fine alignment and stabilization to an atomic reference. Here, we demonstrate both frequency ramping for spectroscopy peak identification and dynamic modulation for generating the spectroscopy locking error signal. The approach to stabilizing the PDH-locked laser to rubidium spectroscopy is shown in Fig. 4(a). We tap a portion of the laser light and send it through a free-space optical rubidium SAS module. We demonstrate locked laser sweeping by applying a 500 Hz voltage ramp to the PIC resonator integrated thermal actuator (Fig. 4(b)) and show that at different DC heater powers the frequency noise of the laser remains unchanged (Fig. S3(a) and Note 3 of Supplement 1). This shifts the cavity resonance, enabling a continuous frequency sweep of the locked laser. The sweep range of over 250 MHz used in this experiment is sufficient to identify the spectroscopic hyperfine peaks within the $F = 2$ manifold based on their relative strengths [35]. We also characterize the dynamic frequency modulation response for generating an error signal to lock the laser frequency precisely to the atomic transition. A small-signal voltage modulation is applied to the thermal actuator, and the frequency response of the locked laser is measured (Fig. S3(b), Supplement 1). While maintaining the lock, we measure the modulation bandwidth (defined at the 180° phase-lag frequency) to be $f_{180^\circ} = 15$ kHz (Fig. S3(c), Supplement 1).

D. Rubidium-Disciplined Resonator

A dual-stage locking approach combines the short-term stability from the ultra-high-Q photonic integrated resonator cavity (PIC) with the long-term absolute frequency stability provided by rubidium spectroscopy (Fig. 4(a)). In the first stage, we PDH-lock a 780 nm DBR laser to the tunable integrated resonator for linewidth narrowing. Prior to engaging the lock, the cavity resonance error signal is tuned by setting the temperature setpoint of the packaged resonator, aligning the resonance to the rubidium $F' = (2, 3)$ crossover transition (Fig. 4(c)). In the second stage, we lock the PIC cavity-stabilized laser to the rubidium SAS signal for long-term frequency referencing. To generate the necessary spectroscopy error signal for atomic locking, we apply a small-signal modulation (9 kHz) to the PIC thermal actuator. This spectroscopy-generated error signal is then fed back to the cavity thermal tuner via a Red Pitaya-based servo loop, to maintain the cavity resonance frequency for robust, long-term alignment with the atomic transition. The inner PDH loop (laser–cavity) is fast compared to the outer Rb-locking loop (cavity–atom), and the large loop bandwidth separation ensures stable nested-loop operation without control interaction.

We next characterize the dual-stage locked laser performance using a combination of the OFD frequency noise system and a cavity-stabilized self-reference optical frequency comb (Fig. 4(a)). The frequency comb (Vescent FFC-100) is disciplined to a Rb frequency standard referenced to a GPS receiver. The comb system generates a beat-note between a frequency-doubled comb line at 780 nm and the locked laser and the beat-note is recorded on a frequency counter. The OFD provides short-term frequency noise at >1 kHz offset frequencies and the comb beat-note is used for <1 kHz offsets long-term drift characterization. The resulting frequency stability time series,

Table 2. Laser Linewidths and ADEV with the Dual-Stage Locked Tunable Integrated Cavity

DBR Laser Lock	$1/\pi$ ILW	β-Separation ILW	ILW Range	ADEV at 1 ms/1 s/10 s
Free-running	182 kHz[a]	5.1 MHz	0.1 Hz to 8 MHz	1.4×10^{-9}/-/-
PIC lock only	246 kHz[a]	306 kHz	0.1 Hz to 8 MHz	$2 \times 10^{-11}/9 \times 10^{-10}$/-
PIC and Rb lock	346 kHz	326 kHz	0.1 Hz to 8 MHz	$8 \times 10^{-11}/8.5 \times 10^{-12}/1.5 \times 10^{-11}$

[a]See footnote in Table 1.

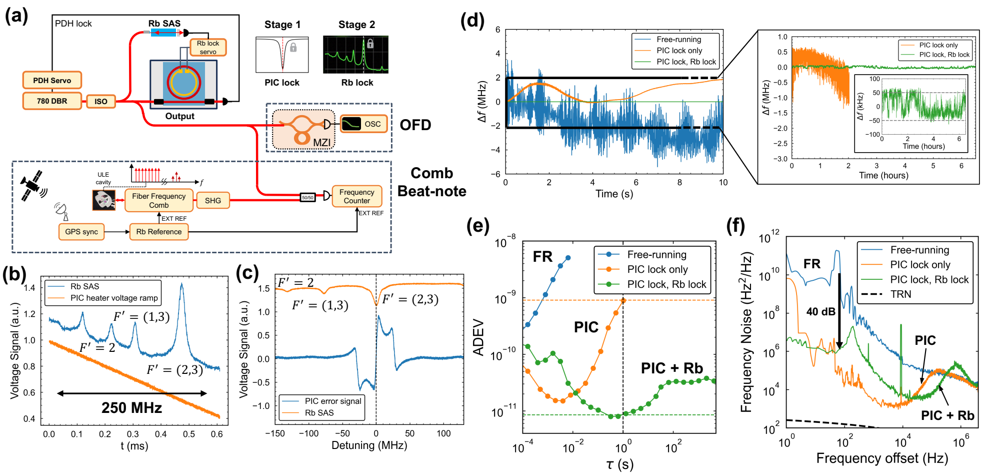

Fig. 4. Dual-stage locking to rubidium spectroscopy. (a) Experimental schematic for the dual-stage locking to the (stage 1) PIC cavity and to spectroscopy (stage 2). The full laser frequency noise and drift is characterized with the optical frequency discriminator (OFD) and ultra-low expansion (ULE) cavity-stabilized fiber frequency comb (Vescent FFC-100) beat-note system. EXT REF, external reference from the SRS FS725 Rb frequency standard; SHG, second harmonic generation. (b) Voltage ramp to the thermal tuner for scanning the locked laser across the rubidium $5S_{1/2}(F=2) \rightarrow 5P_{3/2}(F')$ hyperfine manifold. (c) Aligning PIC error signal and the target spectroscopy resonance. (d) Times series data for the beat-note frequency between frequency-doubled comb line and the dual-stage-locked laser. Inset: The dual-stage locked beat-note signal stays within 100 kHz over the 6 hours of measurement. (e) Allan deviation (ADEV) for different locking conditions: free-running laser, laser locked to the PIC only, laser locked to both PIC and Rb SAS. (f) Frequency noise stitched between the OFD and comb beat-note measurement methods.

Allan deviation (ADEV), and OFD/comb stitched frequency noise data is shown in Figs. 4(d)–4(f) for three different configurations: the free-running DBR laser, the DBR laser locked only to the PIC, and the DBR laser under dual-stage (PIC and rubidium spectroscopy) lock.

The PIC-only lock reduces the short-term laser noise and stabilizes the drift to within several MHz, reducing the free-running laser ADEV by more than two orders of magnitude at millisecond timescales (Figs. 4(d) and 4(e)). However, due to inherent cavity drift, PIC-only locking is insufficient for atomic experiments requiring stable absolute frequency referencing at averaging times greater than 10 ms. The second-stage rubidium spectroscopy lock significantly improves the long-term stability, achieving fractional frequency stability of 8.5×10^{-12} at 1 second averaging time—a two-order-of-magnitude improvement compared to the PIC-only lock performance of 9×10^{-10} at 1 second (Fig. 4(e)). At present, this 1 s instability can be attributed in part to the technical noise in the Rb lock, due to the small error signal slope and the input referred noise of the locking electronics. The dual-stage lock confines the laser frequency drift to within ±50 kHz (RMS fluctuation of 31 kHz) over 6 hours of continuous operation (Fig. 4(d), inset). We attribute the $\tau > 1$ s stability primarily to probe-beam intensity fluctuations in the Rb SAS caused by slow fiber-coupling and polarization drift. Independent probe power logs show 10–20% drift over several hours. Using a measured probe power of 20 μW with 2 μW RMS fluctuations and a light-shift coefficient of ≈10 kHz/μW (scaled from [20]), we expect an RMS frequency fluctuation ≈ 20 kHz.

The frequency noise of the locked laser is shown in Fig. 4(f), with data from two different measurement systems (comb beat-note and OFD) stitched together. At frequency offsets of 100 Hz to 10 kHz, the laser frequency noise increases due to thermal tuner feedback loop in the rubidium SAS lock. The β-separation integral linewidth of the free-running 780 nm laser is reduced from 5 MHz to 306 kHz for the PIC lock only and to 326 kHz for the dual-stage lock. The slight increase in integral linewidth from 306 kHz (PIC-only lock) to 326 kHz (dual-stage lock) is due in part due to the limited bandwidth of the thermal actuator.

Future investigations will focus on improving the actuator performance by linearizing the heater drive, implementing a slow temperature control loop to the resonator TEC, and incorporating MHz-bandwidth stress-optic PZT actuators. To reduce the systematic frequency shifts in the rubidium lock, we also plan to implement an intensity servo to suppress long-term probe beam power fluctuations in the SAS. We summarize the calculated ILWs and ADEV for the different lock loops in Table 2.

3. MULTI-WAVELENGTH RYDBERG SENSING

We demonstrate the use of our tunable integrated resonator to transfer rubidium stability to two lasers in a three-wavelength

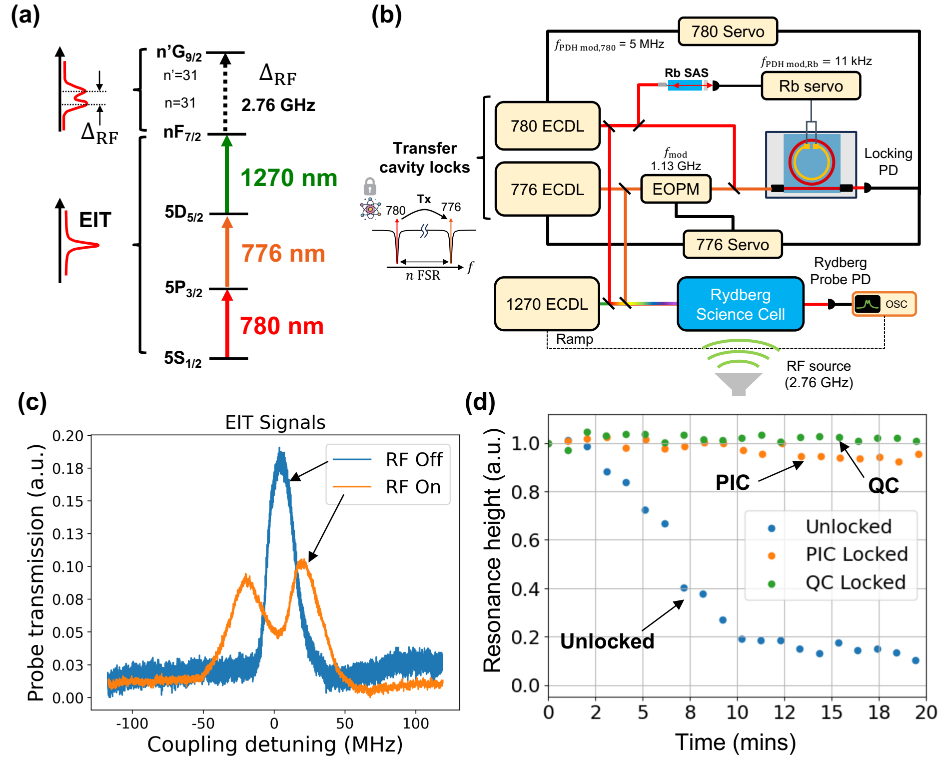

Fig. 5. Simultaneous multi-wavelength locking to PIC reference for three-wavelength Rydberg electrometry for RF field sensing. (a) Energy-level diagram for three-wavelength transition. The alignment of all three optical transitions creates an electromagnetically induced transparent (EIT) signal which is observed by measuring the 780 nm probe laser transmission. (b) Experimental setup for stabilizing the 780 and 776 external cavity diode lasers (ECDL) to the PIC transfer cavity. The 1270 nm coupling laser is scanned through the $|d\rangle \rightarrow |r\rangle 31F_{7/2}$transition and the 780 nm probe transmission is recorded on a photodetector (PD). The 780 ECDL serves as the SAS-locked reference, and the 776 ECDL PDH is PDH sideband-locked to a cavity resonance using an electro-optic phase modulator (EOPM). The external RF source incident at the atoms is operated at 2.76 GHz. (c) 780 probe laser transmission trace as a function of the 1270 laser scan. Strong Autler–Townes splitting is observed when the RF field is on. (d) Rydberg laser transmission signal as a function of time for 780 and 776 lasers free-running (blue), both locked to the Rb-disciplined PIC transfer cavity (orange), and both locked to a table-top quad-bore ULE reference cavity (green).

Rydberg electrometry, where three distinct wavelengths are used to sequentially drive transitions from a ground state to an intermediate excited state and subsequently to a high-lying Rydberg state. Rydberg electrometry allows for measuring RF electric fields with high sensitivity across a wide range of frequencies using room-temperature rubidium vapor cells for precision sensing, RF field mapping, and antenna calibration [11]. The energy diagram for the 780 nm (probe laser), 776 nm (dressing laser), and 1270 nm (coupling laser) is shown in Fig. 5(a). In this application, the long-term stability of the probe and dressing lasers is important to achieving high sensitivity for the RF electric field measurements.

The tunable integrated resonator is used to lock both the 780 nm and 776 nm lasers using a single rubidium spectroscopy reference (Fig. 5(b)). The resonator is critically coupled with high Q resonances over the 776–785 nm range, providing a strong PDH error signal slope for stabilization. We first stabilize a 780 ECDL to the transfer cavity resonator and rubidium spectroscopy using a dual-stage lock (described in the previous section). Next, we stabilize the 776 ECDL to the PIC resonator using electro-optic phase modulator (EOPM) sideband locking, thereby bridging the frequency offset between the cavity resonance and the desired transition frequency and transferring the rubidium-stabilized frequency stability from the 780 nm laser to the 776 nm laser. The details of the lock loop are described in Note 4 of Supplement 1. Finally, the 1270 nm Rydberg coupling laser is scanned through the expected Rydberg transition frequency, while the transmission of the 780 nm probe beam is monitored to detect electromagnetically induced transparency (EIT) signals corresponding to Rydberg excitation (Fig. 5(c)). With a 2.76 GHz RF field incident on the atoms, we observe clear Autler–Townes splitting of the Rydberg resonance, from which the RF electric field amplitude can be derived.

The Rydberg EIT signal (RF off) from the 1270 laser transmission scan is continuously sampled for 20 minutes (Fig. 5(d)). We quantify the signal quality from the trace as a function of time for three different locking conditions: both 780 nm and 776 nm lasers free-running, both lasers locked to the PIC transfer cavity, and both lasers locked to a table-top vacuum-gap ultra-low expansion (ULE) quad-bore reference cavity. The details of the EIT signal data processing are discussed in Note 4 of Supplement 1. We show that locking both lasers to the PIC-based transfer cavity significantly enhances the Rydberg EIT signal stability relative to the free-running condition and achieves comparable performance to that of the ULE quad-bore cavity. To further support these findings, we evaluated the frequency stability of the PIC-based transfer cavity lock using the comb beat-note measurement system (shown in Fig. 3(a)), as discussed in Note 4 of Supplement 1 . The corresponding ADEV traces (Fig. S4(b), Supplement 1) show that both lasers exhibit sub-10^{-10} stability at 1–100 ms averaging times when locked to the PIC. At longer averaging times, the addition of rubidium spectroscopy feedback to the 780 nm laser further disciplines the cavity, reducing the ADEV of the transfer-locked 776 nm laser by nearly an order of magnitude at $\tau = 0.1$ s. The frequency noise at 1 kHz offset was reduced by 20 dB (Fig. S4(c), Supplement 1).

We also confirm that the same PIC resonator supports a 2.2 M loaded Q TE resonance at 1270 nm—used for Rydberg state coupling—suggesting that this wavelength could also be stabilized using the PIC (Fig. S1(d), Supplement 1). While the 1270 nm laser was scanned rather than locked in this work, future implementations could benefit from fully stabilizing all three lasers, especially when the 1270 nm beam serves as a fixed-frequency probe or sensing reference. These results validate the integrated transfer cavity approach for robust multi-wavelength stabilization, demonstrating its suitability for high-precision atomic and quantum experiments. The PIC-based cavity provides a compact and scalable approach to relative laser frequency control and reduces the need for separate atomic references for each laser, expensive fiber frequency combs, or table-top ULE reference cavities.

4. DISCUSSION AND CONCLUSION

In this work, we present a photonic-integrated approach to perform key steps used in the preparation and measurement of atomic states in quantum experiments. These steps include spectroscopy of the atomic hyperfine structure, stabilizing a primary laser and a reference cavity to a desired atom transition, transferring the stability of the atom to additional laser frequencies using additional cavity resonances, performing state preparation of the atom population using the atomically stabilized set of lasers, and making a quantum measurement using a cavity referenced laser. Using a thermally actuated CMOS-foundry-fabricated tunable silicon nitride resonator, we realize a tunable locked laser source with 22 dB of frequency noise reduction at 10 kHz offset and scanning rubidium spectroscopy using precise control of the locked low noise laser frequency. After spectroscopy sweeping, we are able to choose the desired hyperfine transition and implement a dual-stage lock that combines the short-term stability of the integrated resonator with the long-term stability of the rubidium D_2 transition, achieving a fractional frequency stability of 8.5×10^{-12} at 1 second and maintaining frequency drift to within 100 kHz for over 6 hours of continuous operation. We then use the same resonator to transfer the rubidium stability to a second laser and perform quantum atomic state preparation enabling electromagnetic field measurement in a three-wave Rydberg RF sensing experiment. The ability to successfully perform EIT detection on the probe light demonstrates that the rubidium-disciplined cavity resonances provide the required frequency stability for the second laser.

Previous demonstrations of rubidium-disciplined crystalline WGM resonators have achieved excellent frequency stability, reaching $\approx 8 \times 10^{-13}$ at 1 s using self-injection locking combined with piezoelectric actuation [18]. We provide a comparison of WGM results and our SiN work in Table S2 and Note 5 in in Supplement 1. For comparison, passive ULE reference cavities can achieve fractional frequency instabilities approaching 10^{-15} at 1 s with drift rates on the order of kHz/day [37]. While the absolute instability reported here is higher, our work targets atomic-referenced laser stabilization on a CMOS-foundry silicon-nitride platform, enabling wafer-scale reproducibility and operation as a compact, fiber-packaged stabilization module for a variety of lasers. In separate work using the same SiN resonator geometry, we demonstrated self-injection locking with substantially reduced frequency-noise levels [38], which, when combined with the dual-stage atomic lock, can potentially extend the $1/\sqrt{\tau}$ white-frequency-noise region for a lower minimum Allan deviation. Further improvements at averaging times beyond 1 s are expected from tighter control of Rb-related systematic shifts.

Looking forward, this approach can be applied to wide range of neutral atom and trapped-ion experiments that involve broader wavelength spectroscopy and coverage, narrower linewidth atomic transitions, and precision frequency metrology. Examples include probing the rubidium two-photon transition for optical atomic clocks [39,40], trapped ion qubits [41], and multi-wavelength stabilization for polyatomic molecule experiments with many repump wavelengths [42]. While the Rydberg electrometry was performed with a warm vapor cell, a similar stabilization architecture can be extended to cold-atom Rydberg architectures that require narrower laser linewidths [14]. Future work will also focus on simultaneous common-mode beat-note measurements to precisely quantifying the transfer of frequency noise and stability in the multi-laser stabilization across a broader range of resonances and using longer cavities with smaller FSR.

The atomic-disciplined reference and transfer cavity operation offers a compact alternative to traditional table-top multi-bore ULE cavities, costly frequency comb systems, and reduces the need to use multiple atomic references. The agile integrated cavity overcomes limitations of table-top bulk-optic references, namely lack of agility, large free spectral range, and difficulty in planar photonic integration. Beyond the compact footprint and linewidth narrowing capabilities, photonic integrated resonators provide a scalable solution to support significantly lower FSR designs; for example, meter-scale coil resonators on a chip can provide FSRs in the range 10—100 MHz [23,43–45]. In our experiment, the 5.5 GHz FSR cavity required the use of EOPM sideband locking to bridge the gap between the cavity resonance and the desired transition frequency. Reducing the resonator FSR increases the density of available lock points, enabling the cavity resonance to be positioned closer to the atomic transition and thereby reducing the required offset locking frequency. Such low-FSR systems would be challenging to realize using bulk-optic cavities, which would be challenging to fabricate, thermally tune, and stabilize at comparable cavity lengths. Moreover, the integration of stress-optic tuning actuators, such as PZT-on-SiN, enables >10 MHz bandwidth actuation [29–31] and provides fast, chip-scale tuning that overcomes the kHz-level bandwidth limits imposed by mechanical resonances in traditional table-top PZT-actuated cavities, while offering low power (10 s of nW) actuation complementary to thermal tuning. In low-FSR resonator architectures the required offset frequency can therefore be reduced to the 10 MHz regime, where integrated phase modulators, such as ring resonator modulators with demonstrated bandwidths of 20 MHz [29,46] could provide the required modulation directly on-chip. Consequently, integrated cavities with fast, continuous tuning can substantially reduce the reliance on external frequency shifters such as AOMs, which are power consuming and typically limited to a few hundred MHz of tuning range.

Ultimately, co-designing photonic reference cavities with lasers [24,36,38,47,48], modulators [29,30,49], and atomic–photonic interfaces will enable fully chip-integrated quantum systems. This approach can be integrated with on-chip beam delivery, including grating emitters directly coupled to atomic cells for probing and trapping atoms [50,51] to further reduce system size and complexity. Probe-beam intensity stabilization could be implemented on-chip using a Mach-Zehnder interferometer with a phase modulator and photodetectors to actively control the spectroscopy power. These advances highlight the potential of integrated photonic reference cavities as a scalable platform for neutral atom and trapped-ion quantum computing and sensing, ultimately enabling wafer-scale optical systems for timekeeping, navigation, and other quantum technologies.

Funding. DEVCOM Army Research Laboratory (W911NF-22-2-0056), National Aeronautics and Space Administration (80NSSC23K1343), U.S. National Science Foundation (OMA-2016244).

Acknowledgment. We thank Karl D. Nelson at Honeywell for the CMOS fabrication and Jiawei Wang at UCSB for the device metallization. The authors would also like to thank Matthew Hummon and John Kitching at NIST, Joseph Britton and Wance Wang at University of Maryland, and Joshua Hill, David Meyer, and Nathan O'Malley at DEVCOM Army Research Laboratory for useful discussions. We acknowledge Vescent Technologies for their help with setting up the optical frequency comb. This material is based upon work supported by, or in part by, the U. S. Army Research Laboratory and the U. S. Army Research Office under contract/grant number W911NF2310179. The views and conclusions contained in this document are those of the authors and should not be interpreted as representing the official policies, either expressed or implied, of the Army Research Laboratory or the U.S. Government. Any opinions, findings, and conclusions or recommendations expressed in this material are those of the author(s) and do not necessarily reflect the views of the National Aeronautics and Space Administration (NASA).

Disclosures. DJB: ColdQuanta D.B.A. Infleqtion (F, I, C, P). All other authors declare that there are no conflicts of interest related to this article.

Data availability. Data underlying the results presented in this paper are not publicly available at this time but may be obtained from the authors upon reasonable request.

Supplemental document. See Supplement 1 for supporting content.

REFERENCES

1. B. Stray, A. Lamb, A. Kaushik, *et al.*, "Quantum sensing for gravity cartography," Nature **602**, 590–594 (2022).
2. X. Jiang, J. Scott, M. Friesen, *et al.*, "Sensitivity of quantum gate fidelity to laser phase and intensity noise," Phys. Rev. A **107**, 042611 (2023).
3. T. M. Graham, Y. Song, J. Scott, *et al.*, "Multi-qubit entanglement and algorithms on a neutral-atom quantum computer," Nature **604**, 457–462 (2022).
4. J. Kitching, "Chip-scale atomic devices," Appl. Phys. Rev. **5**, 031302 (2018).
5. A. D. Ludlow, M. M. Boyd, J. Ye, *et al.*, "Optical atomic clocks," Rev. Mod. Phys. **87**, 637–701 (2015).
6. C. Audoin, V. Candelier, and N. Diamarcq, "A limit to the frequency stability of passive frequency standards due to an intermodulation effect," IEEE Trans. Instrum. Meas. **40**, 121–125 (1991).
7. C. D. Bruzewicz, J. Chiaverini, R. McConnell, *et al.*, "Trapped-ion quantum computing: progress and challenges," Appl. Phys. Rev. **6**, 021314 (2019).
8. P. O. Schmidt, T. Rosenband, C. Langer, *et al.*, "Spectroscopy using quantum logic," Science **309**, 749–752 (2005).
9. J. A. Sedlacek, A. Schwettmann, H. Kübler, *et al.*, "Microwave electrometry with Rydberg atoms in a vapour cell using bright atomic resonances," Nat. Phys. **8**, 819–824 (2012).
10. N. Thaicharoen, K. R. Moore, D. A. Anderson, *et al.*, "Electromagnetically induced transparency, absorption, and microwave-field sensing in a Rb vapor cell with a three-color all-infrared laser system," Phys. Rev. A **100**, 063427 (2019).
11. D. H. Meyer, Z. A. Castillo, K. C. Cox, *et al.*, "Assessment of Rydberg atoms for wideband electric field sensing," J. Phys. B: At. Mol. Opt. Phys. **53**, 034001 (2020).
12. D. G. Matei, T. Legero, S. Häfner, *et al.*, "1.5 μ m lasers with sub-10 mHz linewidth," Phys. Rev. Lett. **118**, 263202 (2017).
13. E. Pultinevicius, M. Rockenhäuser, F. Kogel, *et al.*, "A scalable scanning transfer cavity laser stabilization scheme based on the red pitaya STEMlab platform," Rev. Sci. Instrum. **94**, 103004 (2023).
14. Y. Zeng, K.-P. Wang, Y.-Y. Liu, *et al.*, "Stabilizing dual laser with a tunable high-finesse transfer cavity for single-atom Rydberg excitation," J. Opt. Soc. Am. B **35**, 454–459 (2018).
15. K. Möhle, E. V. Kovalchuk, K. Döringshoff, *et al.*, "Highly stable piezoelectrically tunable optical cavities," Appl. Phys. B **111**, 223–231 (2013).
16. J. I. Thorpe, K. Numata, and J. Livas, "Laser frequency stabilization and control through offset sideband locking to optical cavities," Opt. Express **16**, 15980–15990 (2008).
17. M. Mäusezahl, F. Munkes, and R. Löw, "Tutorial on laser locking techniques and the manufacturing of vapor cells for spectroscopy," New J. Phys. **26**, 105002 (2024).
18. W. Liang, V. S. Ilchenko, D. Eliyahu, *et al.*, "Compact stabilized semiconductor laser for frequency metrology," Appl. Opt. **54**, 3353–3359 (2015).
19. Y.-H. Lai, D. Eliyahu, S. Ganji, *et al.*, "780 nm narrow-linewidth self-injection-locked WGM lasers," Proc. SPIE **11266**, 78–84 (2020).
20. W. Loh, M. T. Hummon, H. F. Leopardi, *et al.*, "Microresonator Brillouin laser stabilization using a microfabricated rubidium cell," Opt. Express **24**, 14513–14524 (2016).
21. W. Zhang, L. Stern, D. Carlson, *et al.*, "Ultranarrow linewidth photonic-atomic laser," Laser Photonics Rev. **14**, 1900293 (2020).
22. W. Jin, Q.-F. Yang, L. Chang, *et al.*, "Hertz-linewidth semiconductor lasers using CMOS-ready ultra-high-Q microresonators," Nat. Photonics **15**, 346–353 (2021).
23. K. Liu, N. Chauhan, J. Wang, *et al.*, "36 Hz integral linewidth laser based on a photonic integrated 4.0 m coil resonator," Optica **9**, 770–775 (2022).
24. N. Chauhan, A. Isichenko, K. Liu, *et al.*, "Visible light photonic integrated Brillouin laser," Nat. Commun. **12**, 4685 (2021).
25. N. Jin, C. A. McLemore, D. Mason, *et al.*, "Micro-fabricated mirrors with finesse exceeding one million," Optica **9**, 965–970 (2022).
26. L. Maleki, A. Savchenkov, W. Liang, *et al.*, "Miniature atomic clock for space applications," Proc. SPIE **9616**, 190–195 (2015).
27. W. Weng, J. D. Anstie, T. M. Stace, *et al.*, "Nano-Kelvin thermometry and temperature control: beyond the thermal noise limit," Phys. Rev. Lett. **112**, 160801 (2014).
28. L. Cheng, M. Zhao, Y. He, *et al.*, "Spiral resonator referenced low noise microwave generation via integrated optical frequency division," Photon. Res. **13**, 1991–1996 (2025).
29. J. Wang, K. Liu, M. W. Harrington, *et al.*, "Silicon nitride stress-optic microresonator modulator for optical control applications," Opt. Express **30**, 31816–31827 (2022).
30. P. R. Stanfield, A. J. Leenheer, C. P. Michael, *et al.*, "CMOS-compatible, piezo-optomechanically tunable photonics for visible wavelengths and cryogenic temperatures," Opt. Express **27**, 28588–28605 (2019).
31. G. Lihachev, A. Bancora, V. Snigirev, *et al.*, "Frequency agile photonic integrated external cavity laser," APL Photonics **9**, 126102 (2024).
32. A. Isichenko, N. Chauhan, J. Wang, *et al.*, "Tunable integrated 118

million Q reference cavity for 780 nm laser stabilization and rubidium spectroscopy," in *Conference on Lasers and Electro-Optics (CLEO) (2023)* (Optica Publishing Group, 2023), paper SF3K.4.
33. D. J. Blumenthal, R. Heideman, D. Geuzebroek, *et al.*, "Silicon nitride in silicon photonics," Proc. IEEE **106**, 2209–2231 (2018).
34. S. Gundavarapu, G. M. Brodnik, M. Puckett, *et al.*, "Sub-hertz fundamental linewidth photonic integrated Brillouin laser," Nat. Photon. **13**, 60–67 (2019).
35. D. A. Steck, "Rubidium 87 D Line Data," http://steck.us/alkalidata.
36. D. A. S. Heim, D. Bose, K. Liu, *et al.*, "Hybrid integrated ultra-low linewidth coil stabilized isolator-free widely tunable external cavity laser," Nat. Commun. **16**, 5944 (2025).
37. M. Notcutt, L.-S. Ma, A. D. Ludlow, *et al.*, "Contribution of thermal noise to frequency stability of rigid optical cavity via Hertz-linewidth lasers," Phys. Rev. A **73**, 031804 (2006).
38. A. Isichenko, A. S. Hunter, D. Bose, *et al.*, "Sub-Hz fundamental, sub-kHz integral linewidth self-injection locked 780 nm hybrid integrated laser," Sci. Rep. **14**, 27015 (2024).
39. A. Isichenko, A. Kortyna, N. Chauhan, *et al.*, "Tunable 778 nm integrated Brillouin laser probe for a rubidium two-photon optical atomic clock," in *Conference on Lasers and Electro-Optics (CLEO)* (Optica Publishing Group, 2024), paper SM1R.7.
40. K. W. Martin, G. Phelps, N. D. Lemke, *et al.*, "Compact optical atomic clock based on a two-photon transition in rubidium," Phys. Rev. Appl. **9**, 014019 (2018).
41. J.-R. Chen, T.-H. Suen, C.-Y. Kung, *et al.*, "High stability multiple-frequency cavity locking based on doppler-free optogalvanic calcium ion spectroscopy," Opt. Express **30**, 28170–28181 (2022).
42. N. R. Hutzler, "Polyatomic molecules as quantum sensors for fundamental physics," Quantum Sci. Technol. **5**, 044011 (2020).
43. N. Chauhan, K. Liu, A. Isichenko, *et al.*, "Integrated 3.0 meter coil resonator for λ = 674 nm laser stabilization," in *Frontiers in Optics + Laser Science 2022 (FIO, LS)* (Optica Publishing Group, 2022), paper FM1E.1.
44. B. Li, W. Jin, L. Wu, *et al.*, "Reaching fiber-laser coherence in integrated photonics," Opt. Lett. **46**, 5201–5204 (2021).
45. K. Liu, A. S. Hunter, M. W. Harrington, *et al.*, "Photonic integrated silicon nitride 17-meter-long 250-million-Q coil waveguide resonator," in *Conference on Lasers and Electro-Optics (CLEO)*, (2025), pp. 1–2.
46. A. Isichenko, S. Carpenter, N. Montifiore, *et al.*, "Sub-doppler rubidium atom cooling using a programmable agile integrated PZT-on-SiN resonator," arXiv (2026).
47. J. P. McGilligan, K. Gallacher, P. F. Griffin, *et al.*, "Micro-fabricated components for cold atom sensors," Rev. Sci. Instrum. **93**, 091101 (2022).
48. A. Siddharth, A. Attanasio, S. Bianconi, *et al.*, "Piezoelectrically tunable, narrow linewidth photonic integrated extended-DBR lasers," Optica **11**, 1062–1069 (2024).
49. D. Renaud, D. R. Assumpcao, G. Joe, *et al.*, "Sub-1 volt and high-bandwidth visible to near-infrared electro-optic modulators," Nat. Commun. **14**, 1496 (2023).
50. M. T. Hummon, S. Kang, D. G. Bopp, *et al.*, "Photonic chip for laser stabilization to an atomic vapor with 10^{-11} instability," Optica **5**, 443–449 (2018).
51. A. Isichenko, N. Chauhan, D. Bose, *et al.*, "Photonic integrated beam delivery for a rubidium 3D magneto-optical trap," Nat. Commun. **14**, 3080 (2023).